Interfacial oxygen and nitrogen induced dipole formation and vacancy passivation for increased effective work functions in TiN/HfO_2 gate stacks

C. L. Hinkle,[1,2,a)] R. V. Galatage,[2] R. A. Chapman,[2] E. M. Vogel,[1,2] H. N. Alshareef,[3] C. Freeman,[4] E. Wimmer,[4] H. Niimi,[5] A. Li-Fatou,[5] J. B. Shaw,[5] and J. J. Chambers[5]
[1]*Department of Materials Science and Engineering, The University of Texas at Dallas, Richardson, Texas 75080, USA*
[2]*Department of Electrical Engineering, The University of Texas at Dallas, Richardson, Texas 75080, USA*
[3]*King Abdullah University of Science & Technology, Thuwal 23955-6900, Saudi Arabia*
[4]*Materials Design, Incorporated, Angel Fire, New Mexico 87710, USA*
[5]*Advanced CMOS, Texas Instruments Incorporated, Dallas, Texas 75243, USA*

(Received 20 November 2009; accepted 14 February 2010; published online 9 March 2010)

Effective work function (EWF) changes of TiN/HfO_2 annealed at low temperatures in different ambient environments are correlated with the atomic concentration of oxygen in the TiN near the metal/dielectric interface. EWF increases of 550 meV are achieved with anneals that incorporate oxygen throughout the TiN with $[O]=2.8\times10^{21}$ cm^{-3} near the TiN/HfO_2 interface. However, further increasing the oxygen concentration via more aggressive anneals results in a relative decrease of the EWF and increase in electrical thickness. First-principles calculations indicate the exchange of O and N atoms near the TiN/HfO_2 interface cause the formation of dipoles that increase the EWF. © *2010 American Institute of Physics*. [doi:10.1063/1.3353993]

Understanding all the variables that control the effective work function (EWF) of metal gates on Hf-based gate dielectrics has proven to be a challenging task.[1,2] Doping, capping layers, and anneals have been used to manipulate the metal/dielectric interface and modify the work function.[3–11] Creating significant local dipoles via these techniques can manipulate the electrostatic potentials resulting in near band edge effective work functions. In this letter, rapid thermal anneals are employed to incorporate oxygen throughout TiN/HfO_2 gate stacks. EWF shifts are correlated with the oxygen concentration at the metal/dielectric interface resulting from these anneals and atomistic modeling is applied to elucidate how the distribution of oxygen and nitrogen atoms at the interface affects the electrostatic potential.

Metal oxide semiconductor capacitors were built on p-type silicon with a dopant concentration of 1×10^{17} cm^{-3}. Isolation oxide was grown in a conventional furnace and patterned to define the device active areas. SiO_2 interlayers were thermally grown and etched to varying thicknesses before HfO_2 films were formed by atomic layer deposition followed by a 60 s, 700 °C post-deposition anneal in N_2. To enable a series of oxide thicknesses and to decouple reactions at the top metal/dielectric interface from any changes taking place at the dielectric/substrate interface, the high-*k* film thickness was kept constant at 2.0 nm, while the interfacial SiO_2 film thickness was varied from 1.0–3.0 nm. TiN metal gates of 10 nm thickness were deposited using radio frequency sputtering. Rapid thermal anneals (RTA) were performed in N_2 or 10% O_2 in a balance of N_2 (10% O_2/N_2) at atmospheric pressure for 30 s. Al was deposited as a cladding layer and metal contact prior to gate metal patterning. Sputtered Al was used to improve the back side electrical contact. All devices underwent a 400 °C forming gas anneal (FGA) in 10% H_2 in a balance of N_2 to complete processing. Cation secondary ion mass spectroscopy (C-SIMS) analysis was performed on 10 nm TiN films sputtered *in situ* following a thick amorphous-Si sputter deposition on test wafers. The a-Si film is used to create a starting bottom TiN/Si interface with the lowest possible oxygen contamination. Therefore, the oxygen in these samples is predominately due to the incorporation of oxygen via the anneals. These blanket TiN samples were also capped with Al post-anneal for consistency and direct comparison with the electrical test device samples.

Figures 1(a) and 1(b) show the O concentration in the TiN films as a function of sample depth for each annealing condition. C-SIMS is a SIMS-based, proprietary depth profiling technique that monitors molecular (as opposed to atomic) secondary ions emitted under Cs ion bombardment. The major advantage afforded by C-SIMS is the relative independence of ion yields on matrix composition (matrix effect) that allows for accurate quantification in various films and at interfaces. It is readily apparent that oxygen is incor-

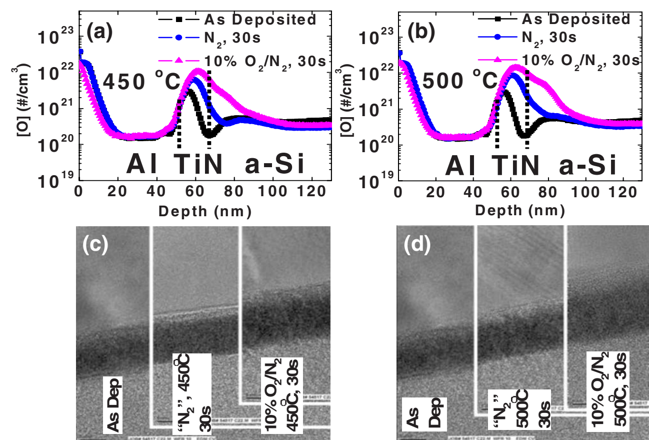

FIG. 1. (Color online) C-SIMS data showing oxygen concentration throughout the TiN films and at the TiN bottom interface for each annealing ambient at (a) 450 °C and (b) 500 °C, while (c) and (d) show TEM cross-sections of the TiN films and interfaces following the anneals.

a)Electronic mail: chris.hinkle@utdallas.edu.

 © 2010 American Institute of Physics

Downloaded 29 Jun 2011 to 137.250.137.85. Redistribution subject to AIP license or copyright; see http://apl.aip.org/about/rights_and_permissions

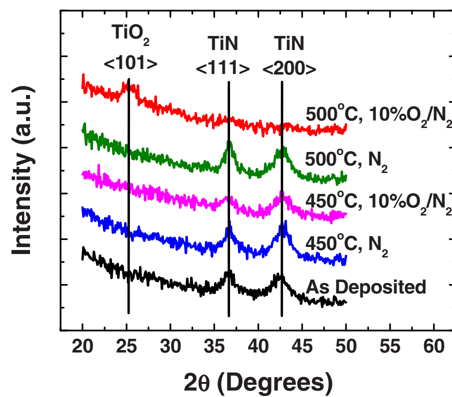

FIG. 2. (Color online) XRD data of blanket TiN films following each annealing condition. No phase change is detectable in the crystal structure except for the 500 °C anneal in 10% O_2/N_2 where the TiN phases are suppressed and a TiO_2 anatase phase arises.

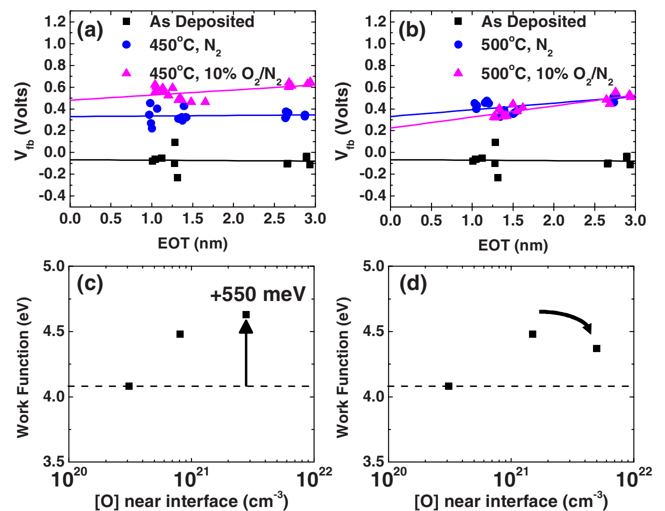

FIG. 3. (Color online) V_{fb} vs EOT plots for TiN/HfO_2 gate stacks for each annealing ambient at (a) 450 °C and (b) 500 °C. The extracted metal gate WFs are plotted as a function of the near interfacial oxygen concentration in (c) and (d). As oxygen concentration increases so too does the EWF except for the structurally changed TiN with a 500 °C anneal in 10% O_2/N_2.

porated during the low temperature anneals. Higher oxygen concentrations are incorporated with increasing temperature. The RTAs were performed in a research grade tool with small traces of residual oxygen present explaining the incorporation of O using N_2 as the ambient gas. Performing the RTAs in 10% O_2/N_2 ambient allowed for the incorporation of greater concentrations of O into the stack as expected. Using the combination of different temperatures and ambients allows for controlling the concentration of oxygen in the TiN with some precision.

Figures 1(c) and 1(d) show the corresponding transmission electron microscopy (TEM) images of the samples after each annealing condition. The images show very little change in the stack for anneals in N_2 ambient compared to the as-deposited films. However, after anneal in 10% O_2/N_2 ambient, the TiN films appear thicker and have undergone intermixing at both the top and bottom TiN interfaces. The TiN in the TEM image corresponding to a 500 °C anneal in 10% O_2/N_2 contains regions of low contrast and regions of lattice fringes indicating the possible conversion of the TiN to TiO_2 in these regions.

Figure 2 shows x-ray diffraction (XRD) data from TiN films exposed to the various anneals. There is no detectable phase change in the TiN between the as-deposited film, the films annealed at 450 °C in either ambient and the TiN annealed at 500 °C in the N_2 ambient. However, the 500 °C anneal in 10% O_2/N_2 ambient shows that the TiN (111) and (200) (Ref. 12) texturing is greatly reduced and that the film now contains TiO_2.

The EWF of each electrode was extracted from plots of flatband voltage (V_{fb}) versus equivalent oxide thickness (EOT) using a series of oxide thicknesses[13] [Figs. 3(a) and 3(b)]. Figures 3(c) and 3(d) combine the extracted EWF from these devices with the interfacial O concentration as determined from the C-SIMS on the samples where the bottom TiN interface was defined at the depth value corresponding to 50% of the rise in Si concentration signal (not shown). The baseline process flow (no RTA after TiN deposition, 400 °C FGA as the final processing step) yields a TiN metal gate with an EWF of 4.1 eV. The oxygen concentration for this baseline process shows an intrinsic level of 3.1×10^{20} cm^{-3}. As the interfacial oxygen concentration increases, the EWF of the TiN also increases. Annealing the gate stacks at 450 °C in the N_2 ambient background increases the interfacial oxygen to $\sim 8.1 \times 10^{20}$ cm^{-3} while the 450 °C anneal in an ambient composed of 10% O_2/N_2 increased the interfacial oxygen concentration to $\sim 2.8 \times 10^{21}$ cm^{-3}. The corresponding EWF values increase by 400 and 550 meV, respectively. The 500 °C N_2 anneal yields an oxygen concentration of $\sim 1.5 \times 10^{21}$ cm^{-3} with a corresponding work function increase in the 400–450 meV range.

Further increasing the oxygen concentration degrades the electrode and the gate stack as a whole. Anneals conducted at 500 °C in an ambient composed of 10% O_2/N_2 increased the interfacial oxygen concentration to $\sim 5.0 \times 10^{21}$ cm^{-3}. This high level of oxygen near the TiN/dielectric interface results in a flattening or even lowering of the EWF as compared to oxygen levels of $\sim 1-3 \times 10^{21}$ cm^{-3}. A concomitant increase in the EOT for these devices and a change in the levels of fixed charge are observed which, when taken in conjunction with the TEM and XRD data, demonstrate that the 500 °C 10% O_2/N_2 anneal is too aggressive. The relative EWF shifts for all conditions were consistent through multiple device runs.

Several interpretations of the associated variation of the EWF and oxygen concentration are possible. For example, oxygen incorporation in TiN may directly change its electronic properties or the substitution of N by O combined with the annealing may cause rearrangements such as filling of vacancies at the interface which lead to changes in the EWF. In order to explore these possibilities, first-principles calculations were carried out to gain a detailed understanding of these mechanisms and their effect on the EWF.

The system was modeled by an interface between the most stable surface of monoclinic $HfO_2(-111)$ and the Ti-terminated TiN(111) surface using the MedeA computational environment.[14] With a hexagonal interface area of 127.4 Å^2 the mismatch in the in-plane lattice parameters is 0.9% and −1.9%. Each of the interface models was fully relaxed by simulated annealing and energy minimization using gradient-corrected density functional theory (DFT) as implemented in the Vienna *ab initio* simulation package (VASP).[15,16] The electrostatic potential corresponding to the self-consistent charge distribution was averaged in planes parallel to the interface

Downloaded 29 Jun 2011 to 137.250.137.85. Redistribution subject to AIP license or copyright; see http://apl.aip.org/about/rights_and_permissions

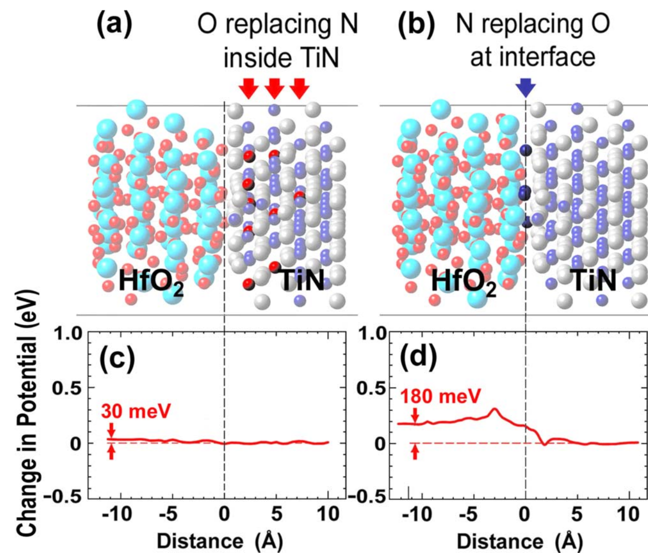

FIG. 4. (Color online) Computed equilibrium structures of HfO_2/TiN interfacial region for (a) O atoms replacing N atoms inside TiN and (b) N atoms replacing 1/3 of the O atoms at the interface. The induced change in the average electrostatic potential relative to the unsubstituted HfO_2/TiN system is shown in (c) and (d). Substitution of N by O inside the TiN layer has a small effect; substitutions of O by N at the interface increase the EWF.

and smoothed by a macroscopic average.[17] The change of this average potential was obtained as the difference between the average potential of the system with atomic substitutions relative to the unsubstituted system.

Substitution of N atoms by O atoms inside the metallic TiN film has only a small effect on the EWF due to metallic screening. For example, by replacing N atoms by O atoms in the layers closest to the interface, the EWF increases only by approximately 30 meV [see Figs. 4(a) and 4(c)]. In contrast, modifications directly at the TiN/HfO_2 interface, i.e., between the interfacial Ti and Hf layers, can change the interface dipole significantly. This is demonstrated for the case when 1/3 of the O atoms at the interface are replaced by N atoms [Figs. 4(b) and 4(d)] which increase the EWF by 180 meV. Replacement of all O atoms at the interface by N increases the EWF by 450 meV. This effect is due to a balance of two opposing dipoles associated with the Ti and Hf atoms at the interface (the sequence O–Hf–O–Ti–N is being replaced by O–Hf–N–Ti–N). Due to the larger polarizability of the Hf atom compared with that of Ti, the dipole associated with the Hf atom is more pronounced creating a net increase of the work function. Furthermore, the filling of oxygen vacancies at one of the twelve O sites at the interface causes an ~80 meV increase in the EWF.

The computational and experimental results suggest the following mechanism. During anneal in an oxygen-containing atmosphere, oxygen atoms penetrate the TiN lattice, fill any N vacancies in TiN and replace N atoms by O atoms. Some of the replaced N atoms are driven toward the TiN/HfO_2 interface where they fill vacancies. C-SIMS analysis suggests the movement of N toward the TiN/HfO_2 interface; however, more detailed physical characterization is required. Nitrogen at the TiN/HfO_2 interface causes a substantial change in the interface dipole such that the electrostatic potential is raised with respect to the Fermi level of TiN, i.e., the Fermi level of the metal gate comes closer to the valence band of the silicon substrate. Overall, the DFT calculations in conjunction with the electrical and physical characterization of the gate stacks demonstrate the importance of controlling the distribution of both oxygen and nitrogen atoms directly at the TiN/HfO_2 interface.

[1] B. H. Lee, J. Oh, H. H. Tseng, R. Jammy, and H. Huff, Mater. Today **9**, 32 (2006).
[2] E. P. Gusev, V. Narayanan, and M. M. Frank, IBM J. Res. Dev. **50**, 387 (2006).
[3] L. Lin and J. Robertson, Microelectron. Eng. **86**, 1743 (2009).
[4] H. J. Li and M. I. Gardner, IEEE Electron Device Lett. **26**, 441 (2005).
[5] J. K. Schaeffer, L. R. C. Fonseca, S. B. Samavedam, Y. Liang, P. J. Tobin, and B. E. White, Appl. Phys. Lett. **85**, 1826 (2004).
[6] E. Cartier, F. R. McFeely, V. Narayanan, P. Jamison, B. P. Linder, M. Copel, V. K. Paruchuri, V. S. Basker, R. Haight, D. Lim, R. Carruthers, T. Shaw, M. Steen, J. Sleight, J. Rubino, H. Deligianni, S. Guha, R. Jammy, and G. Shahidi, 2005 Symposium on VLSI Technology, Digest of Technical Papers, 2005 (unpublished), p. 230.
[7] B. Chen, R. Jha, H. Lazar, N. Biswas, J. Lee, B. Lee, L. Wielunski, E. Garfunkel, and V. Misra, IEEE Electron Device Lett. **27**, 228 (2006).
[8] J. Lee, H. Park, H. Choi, M. Hasan, M. Jo, M. Chang, B. H. Lee, C. S. Park, C. Y. Kang, and H. Hwang, Appl. Phys. Lett. **92**, 263505 (2008).
[9] E. Cartier, M. Steen, B. P. Linder, T. Ando, R. Iijima, M. Frank, J. S. Newbury, Y. H. Kim, F. R. McFeely, M. Copel, R. Haight, C. Choi, A. Callegari, V. K. Paruchuri, and V. Narayanan, 2009 Symposium on VLSI Technology, Digest of Technical Papers, 2009 (unpublished), p. 42.
[10] W. Mizubayashi, K. Akiyama, W. Wang, M. Ikeda, K. Iwamoto, Y. Kamimuta, A. Hirano, H. Ota, T. Nabatame, and A. Toriumi, 2008 Symposium on VLSI Technology, Digest of Technical Papers, 2008, Vol. 42, p. 61.
[11] E. Cartier, M. Hopstaken, and M. Copel, Appl. Phys. Lett. **95**, 042901 (2009).
[12] T. S. Kim, S. S. Park, and B. T. Lee, Mater. Lett. **59**, 3929 (2005).
[13] D. K. Schroder, *Semiconductor Material and Device Characterization*, 2nd ed. (Wiley, New York, 1998), pp. 356–362.
[14] MedeA 2.3, Materials Design, Inc., Angel Fire, NM (2008).
[15] G. Kresse and J. Hafner, Phys. Rev. B **47**, 558 (1993).
[16] G. Kresse and J. Furthmüller, Phys. Rev. B **54**, 11169 (1996).
[17] M. Peressi, S. Baroni, A. Baldereschi, and R. Resta, Phys. Rev. B **41**, 12106 (1990).

Downloaded 29 Jun 2011 to 137.250.137.85. Redistribution subject to AIP license or copyright; see http://apl.aip.org/about/rights_and_permissions